

Supplementary Information

Revealing composition and structure dependent deep-level defect in antimony trisulfide photovoltaics

Weitao Lian^{1,2} Chenhui Jiang^{1,2}, Yiwei Yin¹, Rongfeng Tang¹, Gang Li¹, Lijian Zhang¹, Bo Che¹ and Tao Chen^{1,2*}

¹Hefei National Laboratory for Physical Sciences at Microscale, CAS Key Laboratory of Materials for Energy Conversion, Department of Materials Science and Engineering, School of Chemistry and Materials Science, University of Science and Technology of China, Hefei, Anhui 230026, P. R. China

²Institute of Energy, Hefei Comprehensive National Science Center, Hefei, China

*E-mail: tchenmse@ustc.edu.cn

Supplementary Table 1 Characterisation of the element composition of Sb-rich and S-rich films deposited on soda-lime glass via energy dispersive X-ray spectroscopy (EDS).

Films	Sb at%	S at%	S/Sb	S/Sb (average)
	43.70	56.30	1.29	
	43.90	56.10	1.28	
Sb-rich	43.30	55.90	1.29	1.28
	43.80	56.20	1.28	
	44.10	55.90	1.27	
	38.40	61.60	1.60	
	39.80	60.20	1.51	
S-rich	38.20	61.80	1.62	1.55
	39.90	60.10	1.51	
	39.80	60.20	1.51	

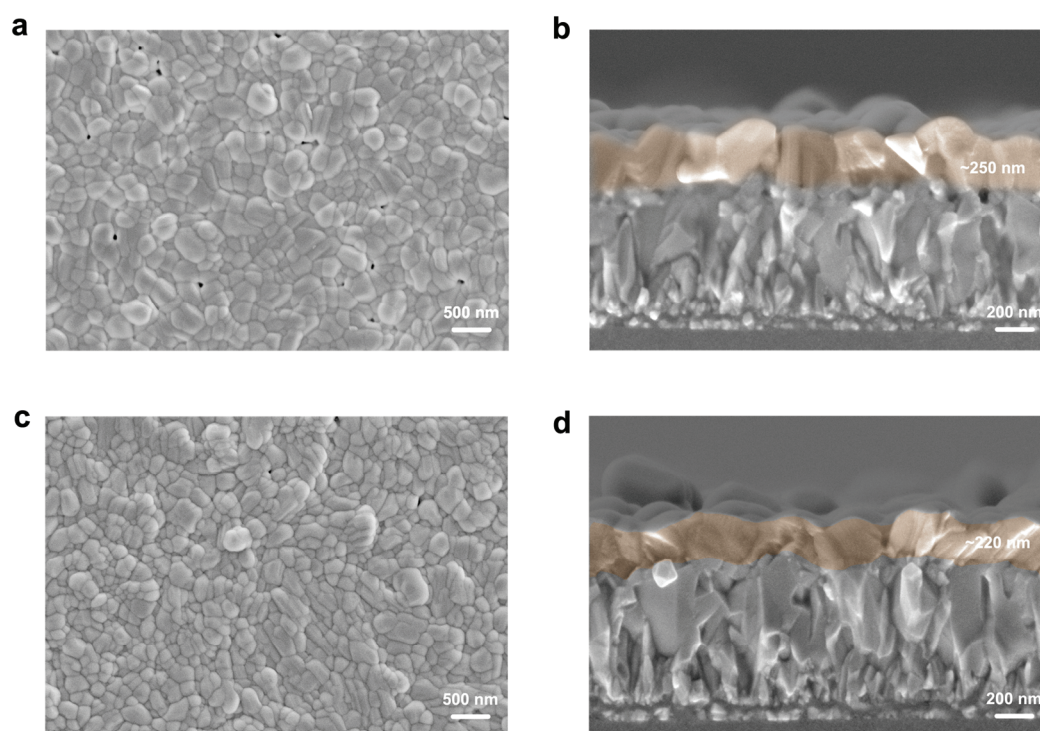
Supplementary Table 2 Fitting results of TAS monitored at 545 nm wavelength.

Films	A_1	$t_1(\text{ns})$	A_2	$t_2(\text{ns})$	$\tau(\text{ns})$
Sb-rich	0.40	0.31	0.60	3.99	3.8
S-rich	0.09	0.38	0.91	18.69	18.7

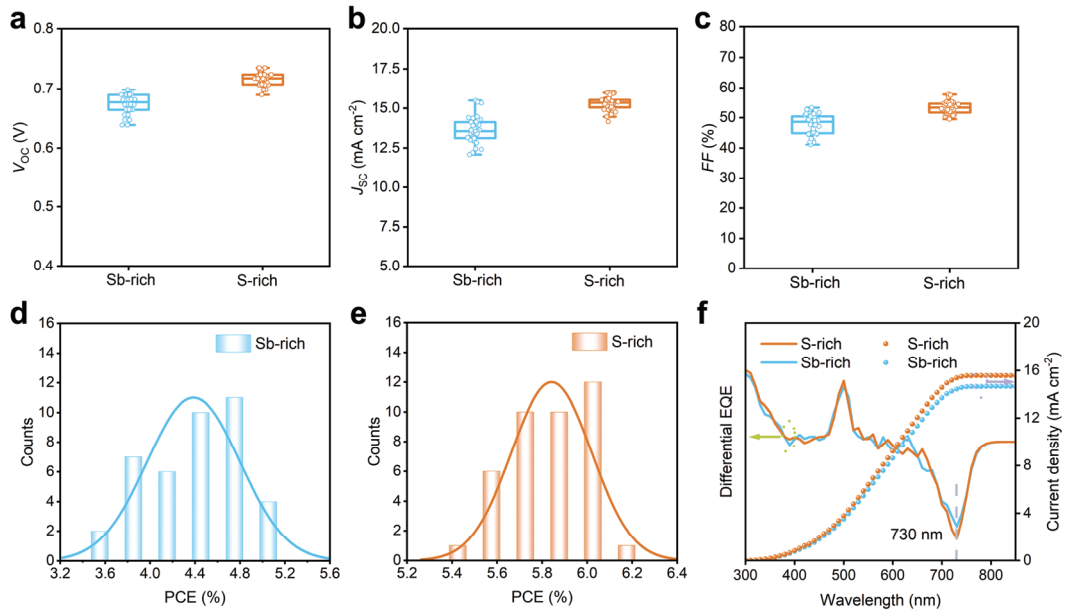
Supplementary Table 3 Photovoltaic parameters of optimal Sb-rich and S-rich Sb_2S_3 devices.

Devices	V_{oc} (V)	J_{sc} ($\text{mA}\cdot\text{cm}^{-2}$)	FF	η (%)	R_s (Ω)	R_{sh} (Ω)
S-rich	0.74*	15.6	52.9	6.1	106.3	6184.6
	0.72	15.9*	54.3*	6.2*	100.4	6677.5
Sb-rich	0.68	15.4	47.6	5.0	116.5	1509.3

(* indicates the champion parameters.)



Supplementary Fig. 1 Films morphology characterizations. **a, b**, Surface and cross sectional morphology of Sb-rich Sb_2S_3 film. **c, d**, Surface and cross-sectional morphology of S-rich Sb_2S_3 film.

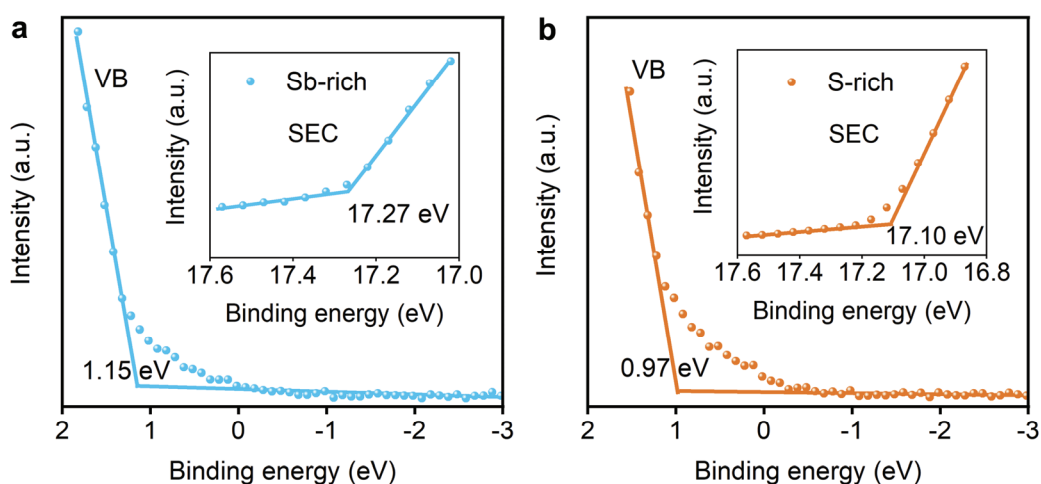


Supplementary Fig. 2 Device photovoltaic performance characterizations. **a-c**, Statistical V_{OC} , J_{SC} and FF based on 40 individually fabricated Sb-rich and S-rich Sb_2S_3 devices. **d, e**, Statistical PCE distribution of 40 Sb-rich and S-rich Sb_2S_3 devices. **f** Differential EQE and integral current density of optimal Sb-rich and S-rich Sb_2S_3 based solar cells.

Supplementary note 1. Ultraviolet photoelectron spectroscopy.

To investigate the dependence of stoichiometry on the work function (Fermi level, E_F) and band structure of Sb_2S_3 films, we carried out ultraviolet photoelectron spectroscopy (UPS) characterizations. According to the secondary electron cutoff (SEC) and valence band (VB) position (Supplementary Fig. 3a and b), the E_F is calculated as -3.95 eV and -4.12 eV, respectively for Sb-rich and S-rich Sb_2S_3 . Furthermore, we find that Sb-rich and S-rich Sb_2S_3 share an identical band gap of 1.70 eV corresponding to 730 nm absorption onset (Supplementary Fig. 2f). Hence, the CBM and VBM are determined to be -3.39 and -5.09 eV for S-rich Sb_2S_3 . The CBM and VBM of Sb-rich Sb_2S_3 film

are -3.40 and -5.10 eV, respectively. Particularly, it is noted that the introduction of S has no impacts on the band structure and band gap but E_F solely. Regarding the downshift of E_F , we attribute it to some reduced shallow donor dopants accompanying with S addition¹. Specially, it is worth noting that the S-rich Sb_2S_3 is still an n type semiconductor even if the E_F shift downward a little after S supplement.



Supplementary Fig. 3 Band structure characterizations. **a, b**, Secondary electron (SEC) cutoff edge and valence band (VB) position of Sb-rich and S-rich Sb_2S_3 films.

Supplementary note 2. DLTS measurement background.

We conduct deep-level transient spectroscopy (DLTS) to detect the deep-level defects properties. The defect level is identified from DLTS signal using Fourier deconvolution algorithm, and Arrhenius plots obtained from defect peaks in DLTS signal are shown in Supplementary Fig. 4. The active energy (E_a , $E_C - E_T$ or $E_T - E_V$) and capture cross section of electron traps and hole traps can be calculated by the Arrhenius equations (1) and (2)²,

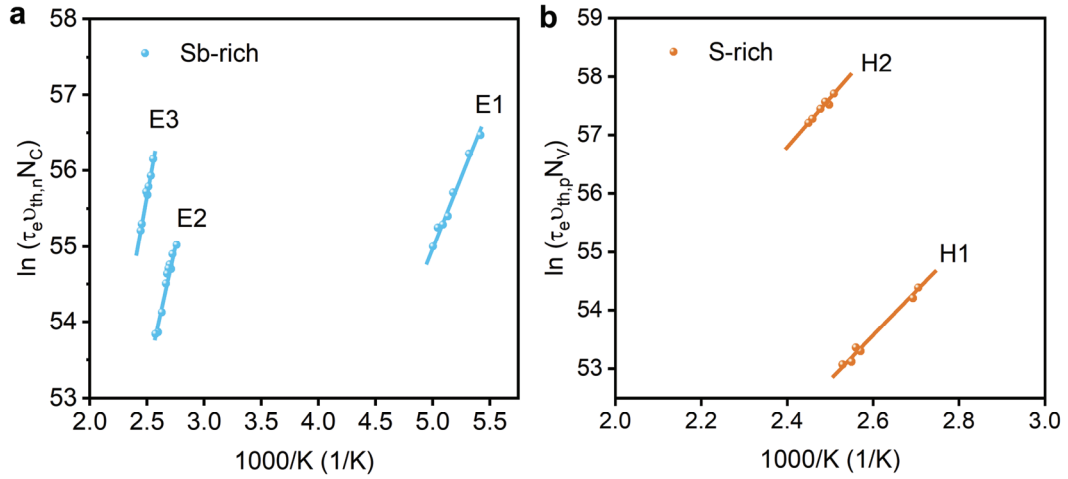
$$\ln(\tau_e v_{th,n} N_C) = \frac{E_C - E_T}{k_B T} - \ln(X_n \sigma_n), \quad (1)$$

$$\ln(\tau_e v_{th,p} N_V) = \frac{E_T - E_V}{k_B T} - \ln(X_p \sigma_p). \quad (2)$$

where τ_e , N_C , N_V , E_C , E_T and E_V are emission time constant, conduction band state density, valence band state density, conduction band, trap energy level and valence band, respectively. $v_{th,n/p}$, $X_{n/p}$ and $\sigma_{n/p}$ represent thermal velocity, entropy factor and capture cross section for electron and hole, respectively. Hence, the E_a and σ can be extracted by the slope and y-axis intercept, separately. In addition, the trap density (N_T) could be obtained by equation (3)²,

$$N_T = 2N_S \frac{\Delta C}{C_R}. \quad (3)$$

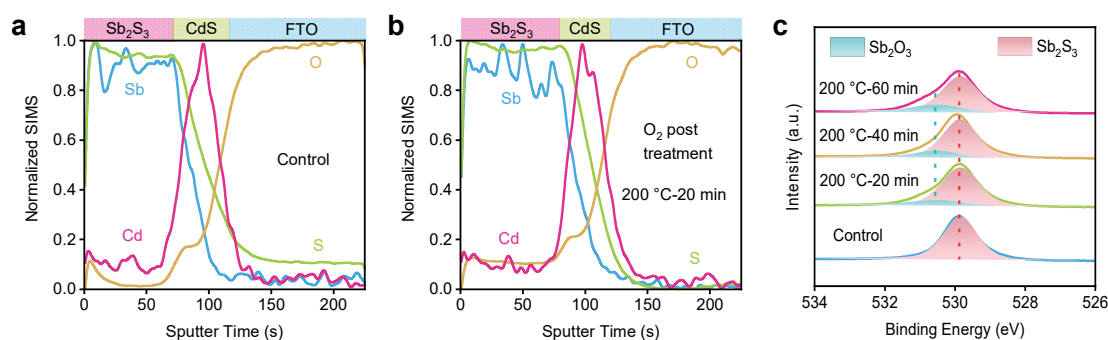
where N_S is the shallow donor concentration, C_R is the capacitance under reverse bias, while ΔC represents the amplitude of transient capacitance.



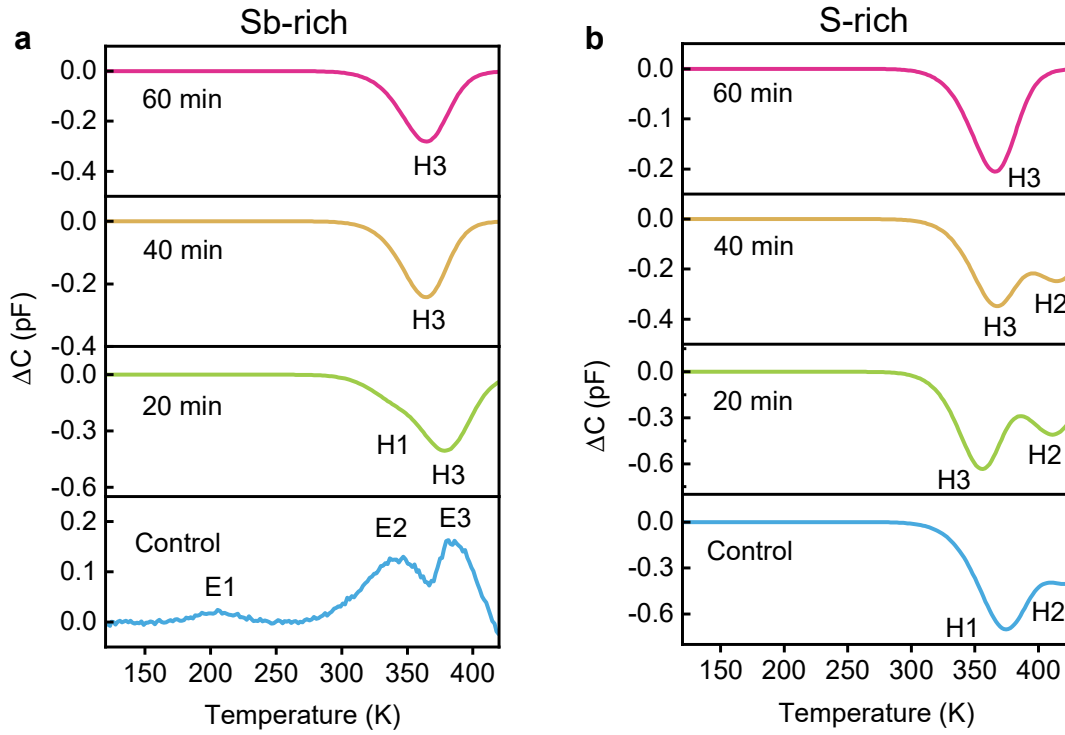
Supplementary Fig. 4 Arrhenius plots obtained from DLTS for Sb-rich (a) and S-rich (b) Sb_2S_3 .

Supplementary note 3. O₂ post-treatment.

To extensively study the influence of low-density oxygen, we adopted O₂ post-treatment for Sb₂S₃ film deposited by thermal evaporation. The as-deposited Sb₂S₃ film was firstly annealed in glovebox as the details described in Methods section (denote as-prepared), then it was placed into a tube furnace to heat at 200 °C for 20, 40 and 60 min in an O₂/Ar (v/v 5%) mixed atmosphere further with a flux of 60 sccm. The heating rate was set as 18 °C per minute, and sample was cooled down to ambient temperature naturally after O₂ post-treatment.



Supplementary Fig. 5 Secondary ion mass spectroscopy (SIMS) and XPS spectra. **a, b**, SIMS of the as-prepared Sb-rich Sb₂S₃ sample (Control) and annealed in O₂/Ar (v/v 5%) at 200 °C for 20 min, respectively. **c** XPS spectra of the as-prepared Sb-rich Sb₂S₃ sample and annealed in O₂/Ar (v/v 5%) at 200 °C for 20-60 min.



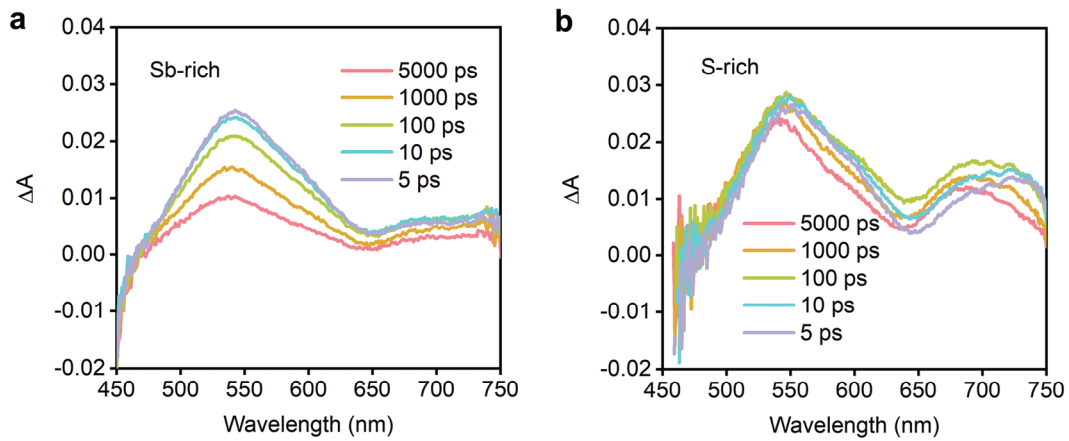
Supplementary Fig. 6 DLTS characterizations. **a**, DLTS characterizations of as-prepared Sb-rich Sb_2S_3 film (denoted as Control) and annealed in O_2/Ar (v/v 5%) at 200 °C for 20-60 min. **b**, DLTS characterizations of as-prepared S-rich Sb_2S_3 film (Control) and annealed in O_2/Ar (v/v 5%) at 200 °C for 20-60 min. The reverse bias, pulse voltage, double pulse (electric & optical) width and period width of DLTS were set as -0.3 V, 0.5 V, 10 ms and 100 ms, respectively.

Supplementary Table 4 The E_T , σ and N_T and N_S extracted from DLTS measurement of as-prepared Sb-rich Sb_2S_3 film (denoted as Control) and annealed in O_2/Ar (v/v 5%) at 200 °C for 20-60 min.

Sb-rich Sb_2S_3	Trap	E_T (eV)	σ (cm²)	N_T (cm⁻³)	N_S (cm⁻³)	
Control	E1	$E_C-0.291$	2.19×10^{-17}	6.07×10^{13}	5.00×10^{16}	
	E2	$E_C-0.621$	6.10×10^{-16}	4.24×10^{14}	5.00×10^{16}	
	E3	$E_C-0.709$	2.00×10^{-15}	6.79×10^{14}	5.00×10^{16}	
O₂ post-treatment	20 min	H1	$E_V+0.612$	3.14×10^{-16}	2.86×10^{14}	2.94×10^{16}
		H3	$E_V+0.674$	1.20×10^{-16}	8.32×10^{14}	2.94×10^{16}
	40 min	H3	$E_V+0.682$	8.45×10^{-16}	1.53×10^{14}	2.63×10^{16}
	60 min	H3	$E_V+0.661$	2.37×10^{-16}	3.29×10^{14}	3.58×10^{16}

Supplementary Table 5 The E_T , σ and N_T and N_S extracted from DLTS measurement of as-prepared S-rich Sb_2S_3 film (denoted as Control) and annealed in O_2/Ar (v/v 5%) at 200 °C for 20-60 min.

S-rich Sb_2S_3	Trap	E_T (eV)	σ (cm²)	N_T (cm⁻³)	N_S (cm⁻³)	
Control	H1	$E_V+0.625$	4.60×10^{-17}	1.42×10^{15}	4.54×10^{16}	
	H2	$E_V+0.759$	1.40×10^{-16}	8.32×10^{14}	4.54×10^{16}	
	20 min	H2	$E_V+0.753$	2.23×10^{-16}	5.88×10^{14}	2.67×10^{16}
O₂ post-treatment		H3	$E_V+0.661$	4.41×10^{-16}	8.72×10^{14}	2.67×10^{16}
	40 min	H2	$E_V+0.730$	9.22×10^{-17}	2.54×10^{14}	2.15×10^{16}
		H3	$E_V+0.669$	2.86×10^{-16}	3.33×10^{14}	2.15×10^{16}
	60 min	H3	$E_V+0.668$	7.70×10^{-16}	3.43×10^{14}	4.62×10^{16}



Supplementary Fig. 7 Carrier transport kinetics. **a, b**, TAS for Sb-rich and S-rich Sb_2S_3 films on soda-lime glass tracked at 5, 10, 100, 1000 and 5000 ps after pulsed excitation at 400 nm.

Supplementary reference.

1. Yin, Y. et al. Composition engineering of Sb_2S_3 film enabling high performance solar cells. *Sci. Bull.* **64**, 136-141 (2019).
2. Lang, D. Deep-level transient spectroscopy: A new method to characterize traps in semiconductors. *J. Appl. Phys.* **45**, 3023-3032 (1974).